# Silicon Nitride Cantilevers for Muscle Myofibril Force Measurements

**CNF Project Number: 1255-04**
**Principal Investigator(s): Walter Herzog**
**User(s): Timothy Leonard, Andrew Sawatsky**

Affiliation(s): Faculty of Kinesiology, University of Calgary, Calgary, Canada

Primary Source(s) of Research Funding: Canadian Institutes of Health Research

Contact: wherzog@ucalgary.ca, leonard@ucalgary.ca, ajsawats@ucalgary.ca
Website(s): https://kinesiology.ucalgary.ca/research/labs-and-centres/human-performance-lab

Primary CNF Tools Used: GCA 5X Stepper, SÜSS MA6-BA6 Contact Aligner, Photolith spinners, Oxford 81 ion etcher

## Abstract:

To measure muscle forces in the nano-Newton range, silicon nitride cantilever pairs were manufactured and used. Measuring sarcomere length (SL) variation across a myofibril with 20-30 sarcomeres in-series in skeletal muscle myofibrils provides useful information about variation in individual SLs and indirectly, the isoform mass, extensibility, and quantity of the structural protein titin [2]. Myofibril imaging has traditionally been done using phase-contrast (PC) microscopy, but this technique has limited resolution. Promising and reliable fluorescent epitope labelling can be done on sarcomeric structural proteins α-actinin (Z-line) and myomesin (M-line).

The purpose of this study was to 1: Test if antibody labelling techniques affect SL non-uniformities and SL repeatability following a stretch-shortening protocol, and 2: Measure passive stress at matched SL to determine if labelling affects passive force development at long SL. Myofibrils from rabbit psoas muscle were used and labelled with anti-α-actinin, anti-myomesin primary antibodies, and polyclonal IgG (H+L) AlexaFluor488 secondary antibodies and observed using both PC and Fluorescein isothiocyanate (FITC) microscopy.

Myofibrils (Labelled, n=7 and Control, n=7) were attached to force-measuring cantilevers and stretched passively from a mean SL of 2.6 $\mu$m (short position; SP) to 3.2 $\mu$m (long position; LP). Fluorescently labelled myofibrils showed no change in the range of SL non-uniformities after stretch compared to non-labelled myofibrils, but labelling contributed to a decrease in individual SL repeatability (as seen in the greater variation around the "perfect" identity line for each sarcomere). Passive force was not affected by the presence of the labels. In conclusion, antibody labeling made SL measurements easier by clearly defining the Z- and M-zones, and while they do not affect the passive force, they do alter the time-history of titin extension during stretch, resulting in poor repeatability of individual SL after stretch-shortening.

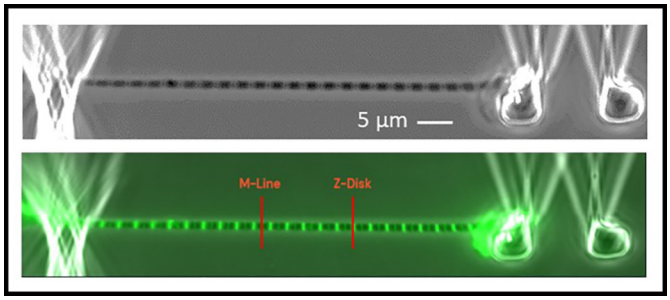


*Figure 1: Myofibril attached to a glass needle for stretch-shortening and nano-cantilevers for force measurement. Top panel is a phase-contrast image and lower panel is the same myofibril, when fluorescently labelled.*

## Summary of Research:

Video images were collected using an Olympus IX83 microscope and analyzed to determine SL in the CellSens® Dimensions software. The maximum number of sarcomeres accurately measurable in each myofibril were chosen, and sarcomeres were pooled together from the seven control and seven antibody-labelled myofibrils, resulting in n=141 control sarcomeres and n=150 antibody-labelled sarcomeres. Individual SL was measured from adjacent M-line centroids throughout the myofibril. SL non-uniformity and individual SL

repeatability were measured after passive stretches, in both control and antibody-labelled myofibrils. An identity line was used for displaying whether each individual sarcomere was the same length, before (x-axis) and after a stretch-shortening test (y-axis). All sarcomeres with perfect repeatability would reside on the identity line. Figure 2 shows the decrease in repeatability in the labelled samples because fewer sarcomeres were close or on, the identity line (x=y).

Force was determined using a microfabricated pair of cantilevers [1], where one end of the myofibril was attached using a mixture of silicon-based adhesive to one of the cantilevers, while the other end of the myofibril was pierced using a glass needle. As passive stretches occurred, the relative movement of the cantilever relative to the stationary cantilever was measured and force calculated based on the known stiffness of the cantilevers. The cross-sectional area of the myofibril was determined and used to determine the stress in the myofibril (nN/$\mu$m$^2$). Figure 3 box plot shows no difference in passive stress at SL of 3.2 $\mu$m.

Overall, the introduction of antibodies did not affect the passive force produced by the myofibril at long SL. It did, however, cause a decrease in the repeatability of the length for each sarcomere following the stretch-shortening cycle. This is possibly due to some "internal drag" caused by the label antibodies or by the fluorophores, on the extension/unfolding of titin during stretch. These findings help support further use of protein labeling in myofibril research.

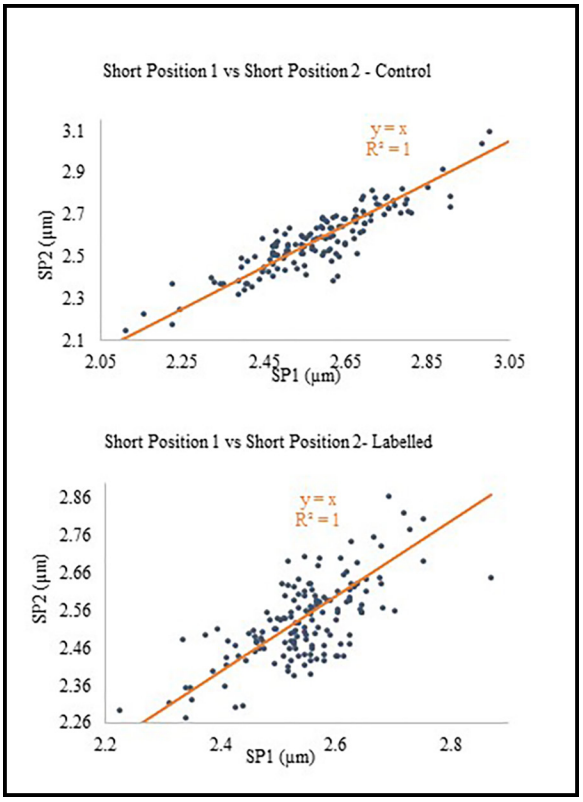


*Figure 2: Sarcomere length for control (top) and labelled (bottom) myofibrils. Each sarcomere was measured prior to stretch (SL on x-axis) and then plotted after stretch-shortening (SL on y-axis). If a sarcomere had the identical length following stretch and return to initial length, then each sarcomere length was perfectly repeatable, and the data point would reside on the "perfect identity line".*

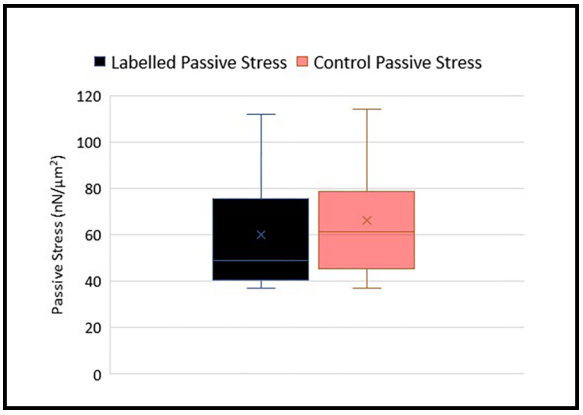


*Figure 3: Boxplots comparing passive stress for control and antibody-labelled myofibrils at long sarcomere length (SL 3.2 µm).*

## References:

[1] M. E. Fauver, et al. IEEE Trans Biomed Eng 45(7):891-898, 1998.
[2] Granzier and Labeit. Muscle Nerve. 36:740-755, 2007.

# High Throughput RF Bio Sensors

**CNF Project Number: 1606-07**
**Principal Investigator(s): Pingshan Wang**
**User(s): Md Saiful Islam**

Affiliation(s): Electrical & Computer Engineering, Clemson University

Primary Source(s) of Research Funding: Army

Contact: pwang@clemson.edu, mdsaifi@clemson.edu

Primary CNF Tools Used: ABM Contact Aligner, SÜSS MA6-BA6 Contact Aligner, CHA Mark 50 E-beam Evaporator, Heidelberg Mask Writer - DWL2000, Glen 1000 Resist Strip

## Abstract:

The aim of this research is to build a microstrip based sensor that has integrated microfluidics to transport biological cells. The sensor will be able propagate low power microwave (100MHz to 15GHz) microwave signals. Biological Cells transported to the sensor will generate electrical signal which will correspond to the dielectric material change. This sensor will be a non-invasive method to analyze biological cells. The sensors are designed to analyze Chinese Hamster Ovarian Cells (CHO) for a comprehensive study of the cell life cycle, different drug effects, conditions effecting the production of protein by the CHO cells, identifying sub-populations that has higher protein yield. Apart from that another set of sensors were built to do similar analysis on candida yeast cells. These investigations will also include SF9 line of cells for cell apoptosis and different virus infection state identification.

## Summary of Research:

The work we did in June 2023 at CNF was to build new devices based on the results obtained earlier this year. In Figure 1, we achieved to demonstrate scattering parameter signals differentiate two different variants of Chinese Hamster Ovarian (CHO) cells. Namely VRC01 and PF variants. In that experiment about 50 individual CHO cells of each type were measured by the sensor (one at a time). Their corresponding scattering parameter scatter plot showed a noticeable difference. However, the sensor had inherent design flaws as in the metal used for the microwave circuit used copper, which would corrode over time and render the sensor unusable. Apart from that the idea of having multiple channel passes with the microfluidic system did not offer any benefits. To remedy this, we came up with some modifications in the microfluidics and planned on changing the metal deposition to Ti-Au-Ti. Some delay line fluidic channel and cell trapping mechanisms were introduced in the microfluidics. The new design has been fabricated over June. We are preparing to run experiments with it on biological cells like CHO, SF9, and candida yeast cells.

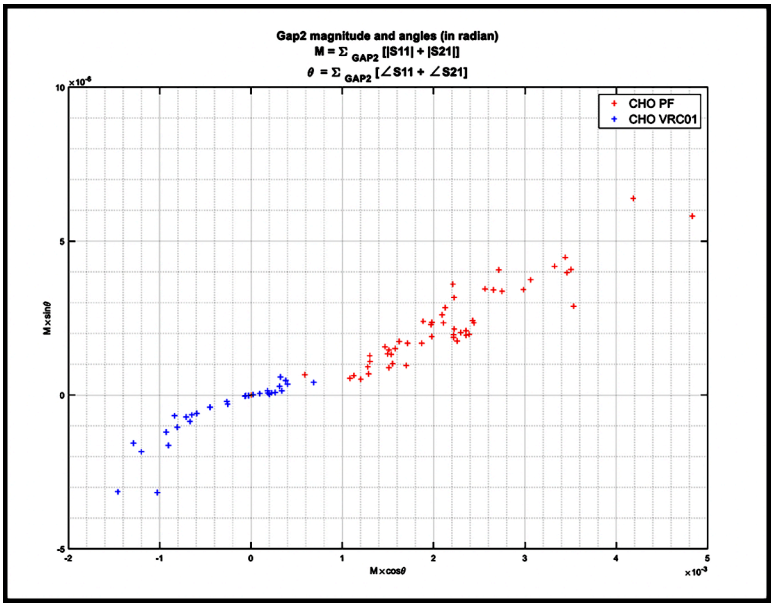


*Figure 1: Scattering parameter scatter plot of CHO VRC01 and CHO PF cells.*

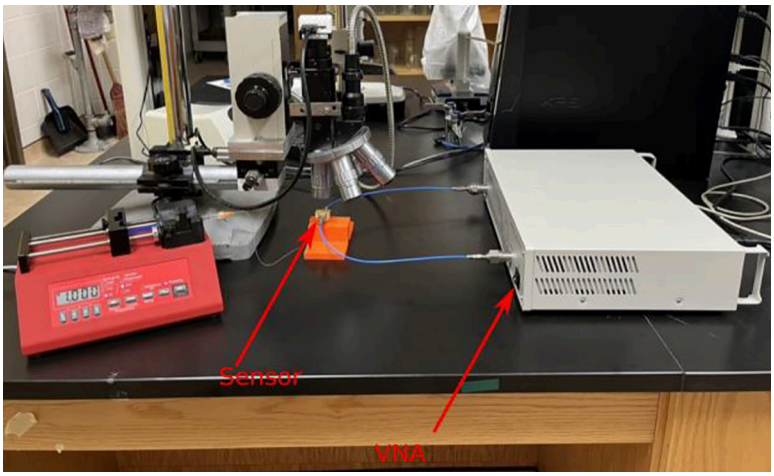


*Figure 2: Experimental setup for the results obtained in Figure 1.*

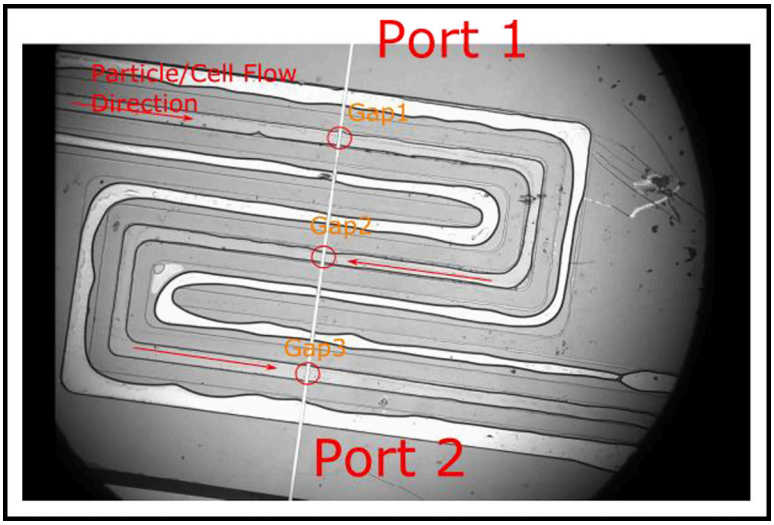


*Figure 3: Microscopic view of microfluidics of the sensor used in Figs 1 and 2.*

# Quartz Cylinder Fabrication for Torque Measurement in the Single-Molecule Level

**CNF Project Number: 1738-08**
**Principal Investigator(s): Michelle D. Wang**
**User(s): Yifeng Hong**

Affiliation(s): a) Department of Electrical and Computer Engineering, Cornell University; b) Department of Physics, Cornell University; c) Howard Hughes Medical Institute

Primary Source(s) of Research Funding: Howard Hughes Medical Institute

Contact: mdw17@cornell.edu, yh874@cornell.edu

Website(s): http://wanglab.lassp.cornell.edu/

Primary CNF Tools Used: ASML Deep Ultraviolet Stepper, Oxford 81 Etcher, Oxford 82 Etcher, Oxford PECVD, SC4500 Odd-Hour Evaporator, SC4500 Even-Hour Evaporator, Zeiss Supra SEM, Zeiss Ultra SEM

## Abstract:

To facilitate single-molecule torque measurements with the angular optical tweezer (AOT), we designed and fabricated quartz cylinders that can specifically attach DNA molecules to achieve a true angular trap. These cylinders have been widely used to investigate single-molecule torsional properties and they are currently uses in multiple research projects.

## Summary of Research:

Torsional stress plays an important role in fundamental biological processes such as transcription and replication. During these processes, torsion can accumulate both upstream and downstream of the transcription complex or the replisome. We are specifically interested in how the DNA responds to these topological changes. To quantitatively investigate this, our lab developed a tool, the angular optical trap (AOT), to measure torque at the single-molecule level [1-3]. In our approach, a linearly polarized light is used to trap and rotate a birefringent particle anchored with a torsionally constrained DNA molecule for manipulations and measurements [1]. To achieve a true angular trap, we designed the birefringent particle to have a cylindrical geometry (with an aspect-ratio ~ 2) [2, 3] (Figure 1). In this way, the cylindrical axis tends to align to the laser propagation direction, which ensures the extraordinary axis is always perpendicular to the laser propagation direction even when attached to a biomolecule. The cylinder top surface is specifically functionalized with (3-Aminopropyl)triethoxysilane to be covalently coupled with protein for DNA molecule anchoring. These quartz cylinders have been broadly used in the single-molecule torsional mechanics study in our lab [3-8].

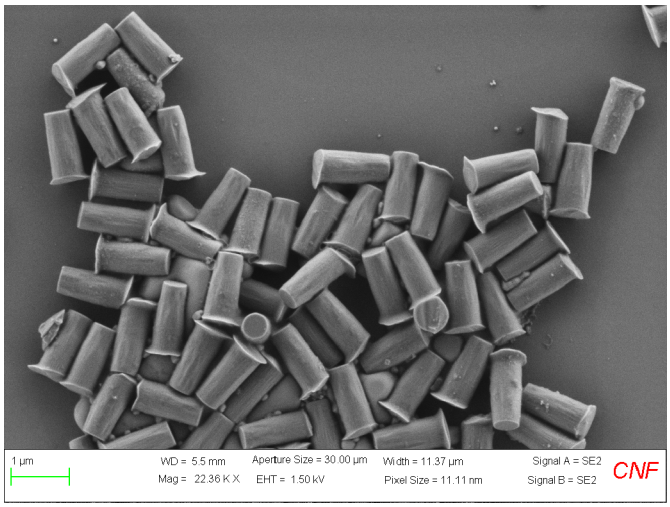


*Figure 1: An SEM image of the cleaved quartz cylinders.*

## Conclusions and Future Steps:

We are now applying the quartz cylinders to extend our previous work on the torsional stiffness of the braided DNA molecules [6].

## References:


[1] La Porta, A. and M.D. Wang, Optical Torque Wrench: Angular Trapping, Rotation, and Torque Detection of Quartz Microparticles. Physical Review Letters, 2004. 92(19): p. 190801.

[2] Deufel, C., et al., Nanofabricated quartz cylinders for angular trapping: DNA supercoiling torque detection. Nature Methods, 2007. 4(3): p. 223-225.

[3] Gao, X., et al., Torsional Stiffness of Extended and Plectonemic DNA. Physical Review Letters, 2021. 127(2): p. 028101.

[4] Forth, S., et al., Abrupt Buckling Transition Observed during the Plectoneme Formation of Individual DNA Molecules. Physical Review Letters, 2008. 100(14): p. 148301.

[5] Ma, J., L. Bai, and M.D. Wang, Transcription under torsion. Science, 2013. 340(6140): p. 1580-3.

[6] Le, T.T., et al., Synergistic Coordination of Chromatin Torsional Mechanics and Topoisomerase Activity. Cell, 2019. 179(3): p. 619-631.e15.

[7] Ma, J., et al., Transcription factor regulation of RNA polymerase's torque generation capacity. Proceedings of the National Academy of Sciences, 2019. 116(7): p. 2583-2588.

[8] Sheinin, M.Y., et al., Torque modulates nucleosome stability and facilitates H2A/H2B dimer loss. Nature Communications, 2013. 4(1): p. 2579.

# Building Microfluidics Devices to Study Zinc Metal Homeostasis in *E. coli* Communities

**CNF Project Number: 1844-09**
**Principal Investigator(s): Peng Chen**
**User(s): Felix Alfonso**

Affiliation(s): Department of Chemistry and Chemical Biology, Cornell University

Primary Source(s) of Research Funding: National Institutes of Health, National Institute of General Medical Sciences

Contact: pc252@cornelll.edu, fsa33@cornell.edu

Website(s): http://chen.chem.cornell.edu/

Primary CNF Tools Used: Heidelberg Mask Writer DWL2000, SÜSS MA6-BA6 Contact Aligner, Oxford Cobra ICP Etcher, Plasma-Therm Deep Silicon Etcher, P7 Profilometer

## Abstract:

Microbial life has evolved a set of molecular tools designed to import essential nutrients from the surrounding environment while simultaneously effluxing the excess to prevent harmful toxicity. The aim of this study is to elucidate the role individual bacterial cells play in achieving metal homeostasis at the community level. With this in mind, we engineered a custom microfluidic device that facilitates the controlled growth of *Escherichia coli* (*E. coli*) colonies within well-defined microchambers. These chambers' dimensions are carefully matched to the diameter of *E. coli* cells, thereby allowing for strategic cellular confinement — a critical aspect of our investigative method. The microfluidic devices we employed exhibit dynamic environmental control features, giving us unprecedented power to study and understand the microbial world. Leveraging this, we were able to probe deeper into the nuances of how this miniature bacterial community strikes a balance in their zinc metal homeostasis.

We employed advanced molecular biology techniques to engineer *E. coli* strains equipped with fluorescent protein reporters. This unique genetic modification allowed us to visualize and quantify gene expressions linked to the intricate influx and efflux ion channels, with particular emphasis on those specific to zinc. The insights derived from this study could have profound implications for our understanding of microbial ecosystems and their interactions with the environment.

## Summary of Research:

Zinc, a fundamental micronutrient, is indispensable for all living organisms [1]. It serves vital functions in protein folding, catalysis, and gene regulation [2,3]. An imbalance in zinc levels, either a deficiency or an excess, can trigger substantial alterations in the gut microbiome, thereby resulting in adverse health conditions [4,5]. Microbial life, over time, has developed a specialized suite of molecular mechanisms to efficiently import nutrients from the environment while effluxing excesses, thus preventing toxicity. To regulate these efflux pumps, bacteria modulate the transcription of protein pumps using metal-responsive transcription regulators. These regulators monitor the cellular concentration of metal ions, guiding cells towards achieving an optimal state of metal homeostasis.

Our project is designed to explore and quantify the management of $Zn^{2+}$ within a microbiome, shedding light on the role individual cells assume in establishing community-wide metal homeostasis. We have chosen *Escherichia coli* (*E. coli*) as our model organism to investigate the complexities of community-derived zinc metal regulation. *E. coli*'s natural motility and poor adherence to substrates present challenges for long-duration imaging studies. However, microfluidics technology offers an effective solution, providing a controlled environment conducive to studying bacterial communities [6]. A microfluidic platform permits tight control of the nutrients influx and has been successfully used for long-timescale imaging studies [7].

The microfluidic device employed in our study is engineered with three key components: a gradient generator, channels, and microchambers. The microchambers' depth is tailored to match the diameter of an *E. coli* cell (~1$\mu$m), thereby facilitating the efficient confinement of colonies. The gradient generator was designed with the goals of creating a stable concentration gradient and minimization of convection inside the chambers. The design presented by E. Bernson, and A. Shamloo provided an optimal method to create a stable

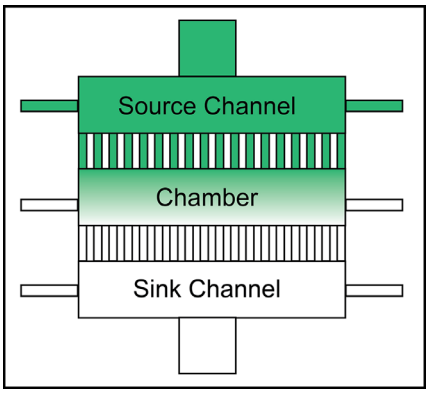


*Figure 1: Schematic of gradient generating microfluidic device showing the source and sink channels and the chamber.*

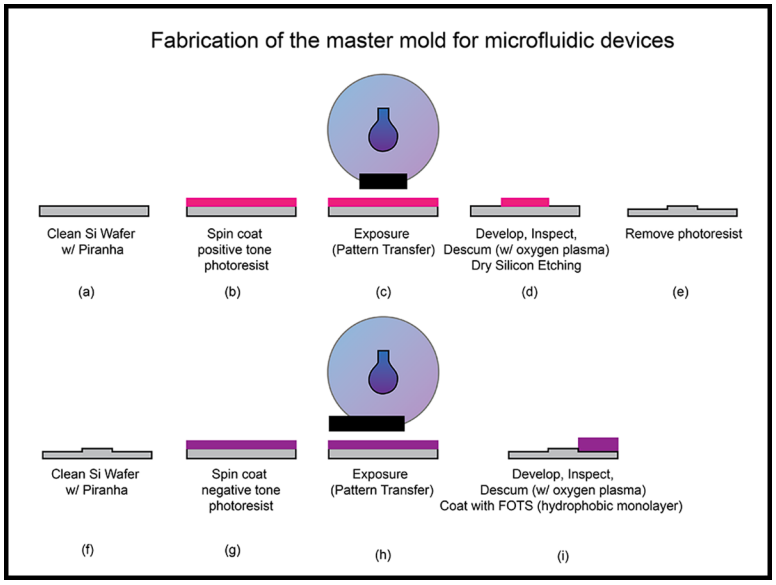


*Figure 2: Fabrication of microfluidic devices combining dry etching to construct the chambers and SU-8 lithography to construct the channels.*

gradient inside the chamber (Figure 1, 8-9). This is accomplished by having a source chamber and a sink chamber. The molecule of interest diffuses through the micro capillaries that connect the source and sink to the main culture chamber.

The construction of these microfluidic devices relies on established silicon nanofabrication technology. The fabrication scheme is summarized in Figure 2. The fabrication process begins with silicon wafers being cleaned with piranha solution. They are then coated with photoresists, which are removed 2 mm from the wafer's edge using an edge bead removal system. The substrate is patterned using a pre-designed photomask created with the Heidelberg Mask Writer DWL2000. The Karl SUSS MA6-BA6 contact aligner provides UV light exposure for the wafer, which is developed and cleaned with a brief oxygen plasma treatment. Chambers are created by etching approximately ~ 1 $\mu$m of silicon using the Oxford Cobra ICP Etcher, and then the photoresist is removed with a stripper bath. The chamber's height is measured using a profilometer. Channel construction involves the use of SU-8 lithography, where SU-8 is spin-coated onto the substrate and patterned with the Karl SUSS MA6-BA6 contact aligner. After a curing phase on a hot plate at 95°C, the unpolymerized SU-8 is removed with the developer. The resulting structure is then hard baked for 10 minutes at 200°C. The final step entails coating the silicon mold with a hydrophobic molecular monolayer such as tridecafluoro-1,1,2,2-tetrahydrooctyl trichlorosilane (FOTS) to facilitate PDMS removal. After casting PDMS on the silicon mold, the microfluidic devices are bonded to coverslips and inspected under a microscope. Cells are loaded into the chambers and imaged with a microscope equipped with the appropriate laser line and filters.

## References:

[1] R. R. Robert B. Saper, Zinc: An Essential Micronutrient. Am. Fam. Physician. 79, 768 (2009).

[2] S. Tan, D. Guschin, A. Davalos, Y.-L. Lee, A. W. Snowden, Y. Jouvenot, H. S. Zhang, K. Howes, A. R. McNamara, A. Lai, C. Ullman, L. Reynolds, M. Moore, M. Isalan, L.-P. Berg, B. Campos, H. Qi, S. K. Spratt, C. C. Case, C. O. Pabo, J. Campisi, P. D. Gregory, Zinc-finger protein-targeted gene regulation: genomewide single-gene specificity. Proc. Natl. Acad. Sci. U. S. A. 100, 11997-12002 (2003).

[3] C. Andreini, I. Bertini, in Encyclopedia of Metalloproteins (Springer, New York, NY, 2013), pp. 2549-2554.

[4] S. R. Gordon, S. Vaishnava, Zinc supplementation modulates T helper 17 cells via its effect on gut microbiome. The Journal of Immunology. 204, 83.18-83.18 (2020).

[5] O. Koren, E. Tako, Chronic Dietary Zinc Deficiency Alters Gut Microbiota Composition and Function. Proc.AMIA Annu. Fall Symp. 61, 16 (2020).

[6] F. Wu, C. Dekker, Nanofabricated structures and microfluidic devices for bacteria: from techniques to biology. Chem. Soc. Rev. 45, 268-280 (2016).

[7] D. Binder, C. Probst, A. Grünberger, F. Hilgers, A. Loeschcke, K.-E. Jaeger, D. Kohlheyer, T. Drepper, Comparative Single-Cell Analysis of Different *E. coli* Expression Systems during Microfluidic Cultivation. PLoS One. 11, e0160711 (2016).

[8] E. Bernson, Development of a Microfluidic Platform for Cell migration Studies along Gradients (2012) (available at https://odr.chalmers.se/items/8199a5e9-f3f0-4824-9056-51f603dcfd7d).

[9] A. Shamloo, N. Ma, M.-M. Poo, L. L. Sohn, S. C. Heilshorn, Endothelial cell polarization and chemotaxis in a microfluidic device. Lab Chip. 8, 1292-1299 (2008).

# Development of 3D Microfluidic Platform for Dynamic Compression of Tumor Spheroids

**CNF Project Number: 2068-11**
**Principal Investigator(s): Dr. Mingming Wu**
**User(s): Young Joon Suh**

Affiliation(s): Department of Biological and Environmental Engineering, Cornell University

Primary Source(s) of Research Funding: NIH Grant R01CA22136,
Cornell Center on the Microenvironment and Metastasis (National Center Institute Grant U54CA143876)

Contact: mw272@cornell.edu, ys668@cornell.edu

Website(s): biofluidics.bee.cornell.edu

Primary CNF Tools Used: Heidelberg Mask Writer - DWL2000, ABM Contact Aligner, P7 Profilometer, MVD100, SUEX Laminator, Dicing Saw - DISCO, YES EcoClean Asher, Unaxis 770 Deep Si Etcher, PT Deep Si Etcher, Oxford 81 Etcher, Oxford PECVD, YES Polyimide Oven, Hamatech Hot Piranha

## Abstract:

Solid tumor stress caused by rapid growth of tumor cells and abnormality of vascular vessels has long been associated with a poor prognosis of cancer. However, understanding of tumor mechanics has been limited largely to single cells under static compressive loads. In this study, we have developed a high throughput microfluidic platform providing well-controlled dynamic compression to tumor spheroids.

## Summary of Research:

A 6 × 2 array microfluidic compression device for tumor mechanics studies was designed (See Figure 1). The device consists of three layers: (1) cell culture layer, where the tumor spheroids embedded in extracellular matrices (ECM) are loaded; (2) PDMS piston layer, which is a PDMS membrane that has a top hat shape; and (3) a pressure control layer, which can push the PDMS piston down to apply compressive forces on the tumor spheroids. The three-layers are then sandwiched between a Plexiglass® top cover and a stainless-steel frame to provide a good seal. A COMSOL modeling has been used to calculate the displacement of the PDMS piston and the force applied on the tumor spheroids at pressure ranging from 0 to 7000 Pa (Figure 2). When pressure is applied in the pressure control chamber, the PDMS piston moves down a distance of Δh, applying a force on the tumor spheroids underneath, and leads to a well-controlled compressive strain, Δh /h, on the spheroids. This device can accommodate tumor spheroids of Young's modulus of about 1250 Pa, that are 100-200 $\mu$m in diameter for up to compressive strain (Δh/h) of 0.5.

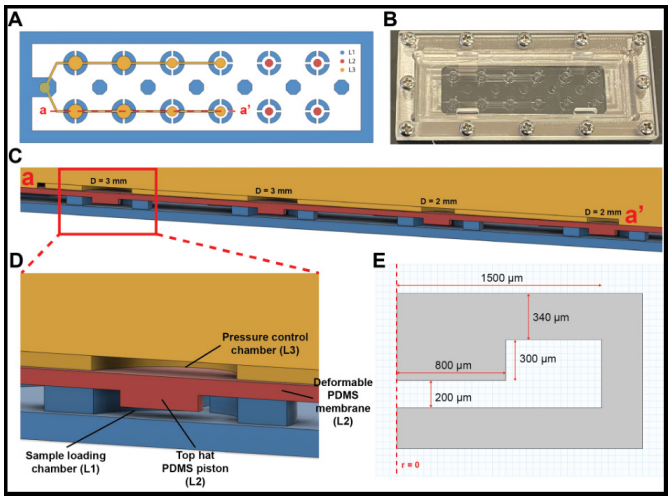


*Figure 1: Design of the Microrheometer. A. Schematic of the three layers L1, L2, and L3. B. Picture of the assembled device. C. Cross-section of the device from a to a'. D. A closeup of the cross-section of one device unit with Sample loading layer (L1), Piston layer (L2), and Pressure control layer (L3). E. Dimensions of an axisymmetric compression unit. A critical dimension is the distance between the bottom of the sample loading well and the PDMS piston, which is 200 µm. The piston layer (L2) has a PDMS membrane thickness of 340 µm, and the piston is 1600 µm in diameter and 300 µm in height. The Sample loading well diameter is 3 mm and 500 µm in height.*

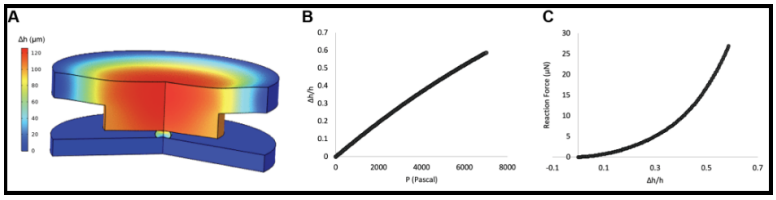


*Figure 2: Computation of a microfluidic compression unit. A. Computed Δh under a pressure of 7000 Pa with spheroid. The spheroid modulus is assumed to be 1250 Pa. B. Relationship between the compression strain and applied pressure. C. Compression force on spheroid versus compression strain, Δh/h.*

## Fabrication:

Three layers of the device were fabricated separately. The cell culture layer consists of SU-8 wells 600 $\mu$m in depth on a 500 $\mu$m thick glass (Borofloat®). To fabricate this layer, SU-8 100 was spun on a Borofloat wafer at 475 rpm and soft baked at 95°C for 30 hours. The SU-8 was then exposed to 2310 mJ/cm$^2$ of UV light through a 365 nm filter using an ABM contact aligner. The resist was then postexposure-baked and developed in the SU-8 developer, followed by a hard bake at 200°C. The main challenge was to fabricate the height of the wells uniform at 600 $\mu$m across the wafer. Keeping the wafer leveled at all steps was found to be crucial. The piston layer consists of PDMS pistons that are 300 $\mu$m in height and 1600 $\mu$m in diameter and the PDMS membrane is 300 $\mu$m thick.

To fabricate the master for this layer, 300 $\mu$m wells were etched into a Si wafer. Briefly, 4.5 $\mu$m of SPR-220-4.5 was spun on a Si wafer. The resist was then baked at 115°C for 2 mins on a proximity hot plate. Then, it was exposed to the pattern of the pistons at 120 mJ/cm$^2$ on the ABM contact aligner. After leaving it in room temperature for 30 mins for the post exposure reaction, it was baked at 115°C for 2 mins on a proximity hot plate for the post exposure bake. It was then developed in 726MIF for 120 sec. Then, a mild descum procedure was completed using the Oxford 81 for 90 sec. Finally, the Si wafer was loaded on the Unaxis 770 Deep Si etcher and a total of 567 loops (200 + 200 + 167) of Bosch process were performed to etch 300 $\mu$m into the Si wafer.

To remove any excess resist, the wafer was exposed to a strong plasma in a EcoClean Asher. The wafer was then coated with FOTS using the MVD-100 to make the surface hydrophobic. The depth of the piston wells was then measured using the P-7 profilometer. The pressure control layer is a PDMS membrane with five parallel channels of 200 $\mu$m depth. The master is fabricated in a similar way as that for cell culture layer, except that a Si wafer is used instead of a Borofloat wafer.

A 10:1 PDMS was poured and cured on the master molds of the piston and the pressure control layer. After curing the PDMS in a 65°C oven overnight, these two layers were bonded together after plasma treatment and placed in a 90°C oven for 20 mins. Then, these two layers were placed on top of the cell culture layer and sandwiched between a metal frame and a Plexiglass top and connected to a pressure controller.

The compression ($\Delta$h) was measured using the defocused particle imaging velocimetry, which was originally developed in our lab [1]. Tumor spheroids were embedded in collagen, which was then introduced into the cell culture chamber. The pressure control chamber is pressurized with a pressure controller. We were able to precisely control the tumor compression with a precision of 1 $\mu$m.

## References:

[1] Wu, et al, Three-dimensional fluorescent particle tracking at micron-scale using a single camera, Experiments in Fluids, 38, 461(2005).

# Microfabrication of Sample Holders for Cryogenic Small Angle X-Ray Scattering and Flow Cells for Fluorescence Measurements of Ligand Diffusion in Protein Crystals

**CNF Project Number: 2157-12**
**Principal Investigator(s): Robert Thorne**
**User(s): John Indergaard, Christopher Biloski, Myeonghak Lee, Ash Mahmood**

Affiliation(s): Departments of Physics, Mechanical and Aerospace Engineering, Cornell University

Primary Source(s) of Research Funding: NIH, NSF

Contact: ret6@cornell.edu, jai55@cornell.edu, cjb358@cornell.edu, ml2564@cornell.edu, km929@cornell.edu

Website(s): https://www.lassp.cornell.edu/Thorne/

Primary CNF Tools Used: Heidelberg DWL 2000 Laser Writer, Hamatech Wafer Processor, Filmetrics Reflectometer, SÜSS MA6 Contact Aligner, Oxford PlasmaLab 80+, SUEX Laminator, Harrick Plasma Generator, PDMS Casting Station, DISCO Dicing Saw, KOH Hood and Bath

## Abstract:

Small angle X-ray scattering (SAXS) and X-ray crystallography are key tools used to study the structure and function of biomolecules. We have been developing microfabricated sample cell arrays for collection of SAXS data from biomolecular samples cooled to cryogenic temperatures, which could simplify SAXS sample handling and increase data collection throughput. We have also been developing microfluidic flow cells for quantitative fluorescence measurements of diffusion of small molecules into biomolecular crystals. These measurements inform choice of crystal sizes in time-resolved crystallography of biomolecules in action.

## Summary of Research:

Sample cell arrays for cryo-SAXS. Small-angle X-ray scattering (SAXS) probes the shape and size of biomolecules (e.g., proteins) in solution. SAXS is currently performed using biomolecule samples at or near room temperature. Samples are rapidly damaged by X-rays and may undergo degradation during transport to the X-ray source. If samples are cooled to cryogenic temperature, the rate of X-ray damage decreases by orders of magnitude and samples can be stored indefinitely without degradation. Our goal is to develop sample cell arrays and methods to enable routine high-throughput SAXS sample handling and measurements at cryogenic temperature. Major challenges in achieving this goal include finding a combination of materials, structures, and protocols that allow easy loading of nanoliter sample volumes, sample cooling into a vitrified state without formation of crystalline ice, bubbles, anisotropic stresses, or fractures, and that allow quantitatively and qualitatively identical data to be collected from any cell in the array.

Our sample cell arrays are constructed from two 3 mm × 12 mm pieces of 300 $\mu$m thick, <100> oriented, double-side polished Si wafer, coated via LPCVD with 500 nm of SiN. The wafer is photolithographically patterned, SiN is removed from one side, and Si is removed using an anisotropic KOH etch, leaving arrays of 500 $\mu$m square, X-ray transparent SiN windows. A sheet of SUEX is bonded to the window side of the wafer and patterned to define cell alignment and liquid trapping features. The wafer is diced into rectangles containing eight windows, each forming half of a sample cell array. On one half, segments of thin-walled polyimide tubing are bonded over each nitride window and quartz spacers are attached. The spacers fix the distance between nitride windows in the two halves of the device, fixing the X-ray path length through each cell.

We have evaluated our cryoSAXS sample cell arrays at synchrotron beamlines at CHESS (Cornell) and NSLS-II (Brookhaven National Lab). The cells allow rapid cooling to a vitrified sample state. The critical challenge has been to eliminate all sources of cell-to-cell variability/irreproducibility in SAXS scatter, as differences as small as 1% can have a major impact on data quality. We have been addressing this challenge via changes in device geometry and assembly, changes in X-ray beamline configuration, and changes in device cleaning protocols.

Our current design — involving both microfabrication and precision manual assembly — presents obstacles to both reproducible data collection and routine, high-volume production and use. We will continue optimization of the current design and exploring alternative designs, including all-microfabrication designs made possible using two-photon polymerization.

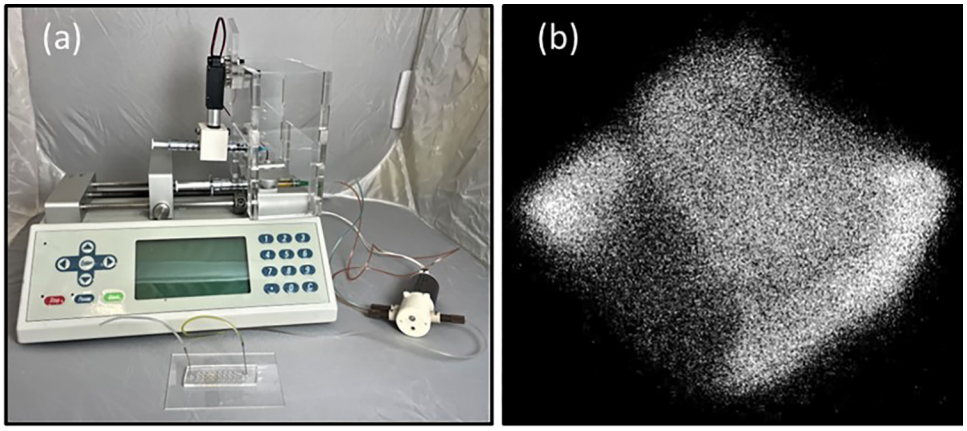


*Figure 1: (a) Experimental setup including microfluidic crystal trap array for measuring diffusion of fluorescent small molecules into biomolecular crystals. (b) Two-photon fluorescence image of a fluorophore (lysotracker blue DND-22) diffused into a ~ 50 µm lysozyme crystal.*

Microfluidic traps for *in crystallo* diffusion measurements. A long-term project in structural biology has been to develop methods for making atomic-resolution "movies" of biomolecules in action. This typically involves mixing small crystals with a ligand that diffuses into the crystal and binds to the biomolecule, reacting with it and/or triggering a change in its structure. X-ray diffraction patterns are recorded at different times after the start of mixing and are used to generate "snapshots" versus time.

We demonstrated a mix-and-quench method [1] where biomolecular crystals on a support are translated through a film containing reactant. After a delay, the crystals are plunged into liquid nitrogen, stopping the reaction and trapping the structural state for subsequent X-ray examination. We achieved a nominal time resolution of 40 ms, and with hardware improvements sub-5 ms time resolution should be feasible.

However, a key unknown is the time required for a given ligand/reactant to diffuse into a given biomolecular crystal. Time-resolved experiments have so far assumed that diffusion constants within crystals are the same as in free solution. However, biomolecular crystals are nanoporous solids with complex internal pore geometries. Diffusion constants could be one to two orders-of-magnitude smaller, causing uncertainty in reaction "time points" due to inhomogeneous ligand distribution within the crystal, limiting achievable time resolution, and/or requiring use of much smaller crystals.

To examine diffusion within crystals, we are fabricating microfluidic flow cells for use in multiphoton imaging (Figure 1). Crystals in carrier solution flow into the cells and are trapped at an array of locations, and then a solution containing a small-molecule fluorophore flows into the cell and diffuses into the crystals. To create these crystal traps, we fabricate a master mold by bonding a SUEX sheet to a silicon wafer and photolithographically patterning it. Trap arrays are fabricated by casting a 2 mm layer of PDMS on top of the wafer. Once the crystal traps are filled by a flow of crystal-containing solution, fluorophore is abruptly introduced using an electronically controlled syringe-holding manifold and a switching valve.

We have demonstrated successful trapping of 50 $\mu$m crystals and obtained fluorescence data yielding a plausible initial diffusion coefficient estimate. We are improving the design to allow study of larger crystals (which should give more accurate estimates) and faster flow switching to improve time resolution.

## References:

[1] Clinger, J. A., Moreau, D. W., McLeod, M. J., Holyoak, T., and Thorne, R.E. Millisecond mix-and-quench crystallography (MMQX) enables time-resolved studies of PEPCK with remote data collection. IUCrJ 8, 784-792 (2021).

# Nanoscribe 3D Printing of Versatile Microfluidic Mixers for Experiments with Biomolecules

**CNF Project Number: 2158-12**
**Principal Investigator(s): Lois Pollack**
**User(s): Scout Fronhofer, Kara Zielinski**

Affiliation(s): Applied and Engineering Physics, Cornell University
Primary Source(s) of Research Funding: National Science Foundation
Contact: lp26@cornell.edu, shf56@cornell.edu, kaz42@cornell.edu
Website(s): https://pollack.research.engineering.cornell.edu/
Primary CNF Tools Used: Nanoscribe 3D Printer

## Abstract:

We report the fabrication and implementation of a 3D printed microfluidic mixer for studying biological macromolecules. The device mixes fluids by chaotic advection, enabling time-resolved structural measurements of large molecules and offers advantages over turbulent mixers in terms of sample consumption. Previous versions of the mixer have been used for time-resolved measurements for multiple biological systems and techniques, and there are many avenues for future work.

## Summary of Research:

Microfluidic mixers have enabled time-resolved structural studies of biological macromolecules [1,2]. Snapshots of the reaction can be captured by different structural techniques, such as X-ray crystallography [3], Small Angle X-ray Scattering (SAXS) [4], and various spectroscopies [5]. Many time-resolved experiments have utilized flow-focused diffusive mixers [2], which rely on an outer sheath flow to thin the central sample stream so small molecules can rapidly diffuse into the stream for reaction initiation. Timescales ranging from single milliseconds to seconds are reachable. One reactant, however, must be relatively small and highly soluble for efficient diffusion. Thus, diffusive mixers are suited for reactions involving one large biological macromolecule, such as a protein or nucleic acid, and one small ligand.

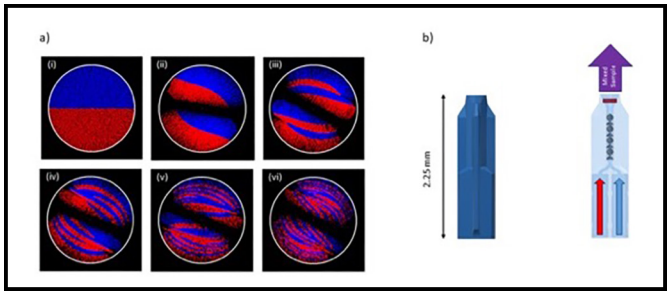


*Figure 1: (a) Cross section of simulated flows after each mixing element inside the Kenics (b) CAD rendering of the exterior and cross section of the Kenics.*

Reactions between two biological macromolecules, such as two proteins or a protein and a nucleic acid, are essential so there is interest in studying these interactions via time-resolved measurements. Turbulent mixers can achieve this, but high sample consumption is often prohibitive for lab-purified biological molecules. Mixing by chaotic advection is a strong alternative to diffusive and turbulent mixers, as the mixing is efficient enough for reactions between large macromolecules, and sample consumption is lower than turbulent mixers. The Kenics is a type of chaotic advection mixer that consists of a channel containing several helical mixing elements (Chemineer, Dayton, Ohio). As two fluids flow through, these mixing elements cause the fluids to undergo baker's transformations (Figure 1a); the two fluids are repeatedly stretched, split, and stacked on top of one another [6], and increasingly thin layers are produced, facilitating the diffusion of molecules between the two fluids. This design has efficient mixing for large molecules and can reach timepoints from 10 ms and beyond.

Kenics mixers can be fabricated using the Nanoscribe 3D printer at CNF. The Nanoscribe uses two-photon polymerization to print with submicron resolution, which is the level of precision required for our design (Figure 1b). The mixer was designed using Autodesk Inventor and the print settings were programmed in Describe. The inserts were printed with IP-S resin and 70% laser power. After printing, the inserts were placed in propylene glycol monomethyl ether acetate (PGMEA) for development for at least four days. Next, the inserts were submerged in IPA and sonicated for five minutes before UV curing for 60 minutes.

Previous versions of this mixer have been used for time-resolved SAXS (TR-SAXS) measurements [7]. Mixers of this design can also be coupled to other measurements. Absorbance spectroscopy was used to track the binding of myoglobin and azide, which caused a shift in the absorbance that was captured over time (Figure 2). The k value of the binding was accurately extracted from this data, demonstrating that kinetics experiments are possible [7]. Recent, CNF fabricated versions of this device are being used for x-ray spectroscopy measurements, with encouraging preliminary results.

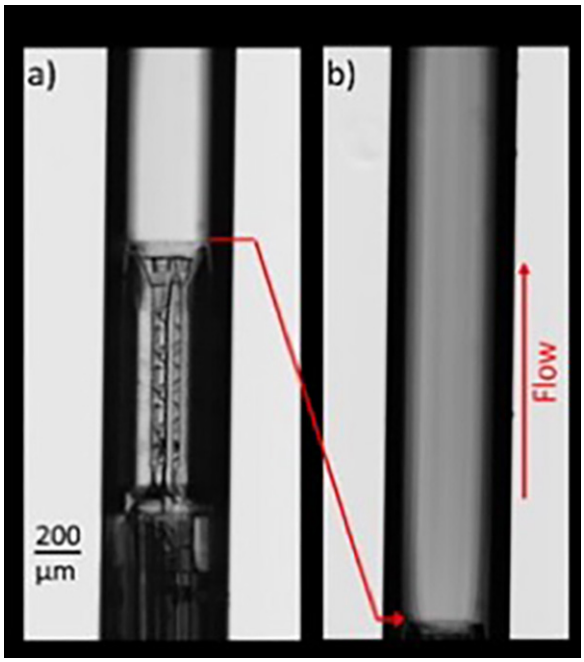


*Figure 2: (a) Kenics mixer inside glass capillary absorbance spectroscopy measurements. (b) Fully mixed myoglobin and azide exiting the Kenics (tip of the mixer moved to the bottom of the field of view).*

## Conclusion and Future Steps:

Due to the high precision of the NanoScribe 3D Printer, we can fabricate a Kenics mixer for time-resolved experiments of a wide range of biological systems and a variety of techniques. Past work demonstrates the utility of this design for probing protein-protein, protein-nucleic acid, protein-ligand, and nucleic-acid ligand reactions with SAXS and absorbance spectroscopy. Future experiments will explore additional biological systems and use other techniques to capture the dynamics of biological reactions.

## References:

[1] Calvey, G. D., Katz, A. M. & Pollack, L. (2019). Anal. Chem. 91, 7139-7144.

[2] Calvey, G. D., Katz, A. M., Schaffer, C. B., and Pollack, L. (2016). Struct. Dyn. 3, 054301.

[3] Olmos, J. L., Pandey, S., Martin-Garcia, J. M., Calvey, G., Katz, A., Knoska, J., Kupitz, C., Hunter, M. S., Liang, M., Oberthuer, D., Yefanov, O., Wiedorn, M., Heyman, M., Holl, M., Pande, K., Barty, A., Miller, M. D., Stern, S., Roy-Chowdhury, S., Coe, J., Nagaratnam, N., Zook, J., Verburgt, J., Norwood, T., Poudyal, I., Xu, D., Koglin, J., Seaberg, M. H., Zhao, Y., Bajt, S., Grant, T., Mariani, V., Nelson, G., Subramanian, G., Bae, E., Fromme, R., Fung, R., Schwander, P., Frank, M., White, T. A., Weierstall, U., Zatsepin, N., Spence, J., Fromme, P., Chapman, H. N., Pollack, L., Tremblay, L., Ourmazd, A., Phillips, G. N., and Schmidt, M. (2018). BMC Biology 16, 59.

[4] Plumridge, A., Katz, A. M., Calvey, G. D., Elber, R., Kirmizialtin, S., and Pollack, L. (2018). Nucleic Acids Research 46, 7354-7365.

[5] Calvey, G. D., Katz, A. M., Zielinski, K. A., Dzikovski, B., and Pollack, L. (2020). Anal. Chem. 92, 13864-13870.

[6] Saatdjian, E., Rodrigo, A. J. S., and Mota, J. P. B. (2012). Chemical Engineering Journal 187, 289-298.

[7] Zielinski, K. A., Katz, A. M., Calvey, G. D., Pabit, S. A., Milano, S. K., Aplin, C., San Emeterio, J., Cerione, R. A. & Pollack, L. (2023). IUCrJ 10, 363-375.

# Metasurface-Enhanced Infrared Spectroscopy for the Measurement of Live Cells

**CNF Project Number: 2472-16**
**Principal Investigator(s): Gennady Shvets**
**User(s): Steven He Huang, Po-Ting Shen, Aditya Mahalanabish**

Affiliation(s): Applied and Engineering Physics, Cornell University

Primary Source(s) of Research Funding: National Cancer Institute of the National Institutes of Health award number R21 CA251052. National Institute of General Medical Sciences of the National Institutes of Health award number R21 GM138947

Contact: gs656@cornell.edu, hh623@cornell.edu, ps944@cornell.edu, am2952@cornell.edu

Website(s): http://shvets.aep.cornell.edu

Primary CNF Tools Used: JEOL 9500, SC4500 evaporator, Zeiss Supra SEM, PDMS Casting Station, Anatech Resist Strip, Glen 1000, Oxford PECVD, Oxford ALD FlexAL, Plasma-Therm 720/740, DISCO dicing saw

## Abstract:

We have developed Metasurface-Enhanced Infrared Spectroscopy (MEIRS) as a novel tool to perform spectral analysis and chemical imaging of live cells. In MEIRS, cells are cultured on an array of plasmonic nanoantennas (metasurface), which enhances infrared vibrational signal through the coupling of molecular vibrations to plasmonic resonances. Various cellular responses can be observed from the infrared spectra collected in real-time. Our current work focuses on expanding the application of MEIRS to the chemical imaging of live cells as well as combining plasmonic metasurfaces with nano-topography to study cell-nanostructure interactions.

## Summary of Research:

Infrared (IR) spectroscopy is widely used to identify chemical compounds through their molecular vibration fingerprints and has recently found many applications in biological analysis. We have developed a novel technique called Metasurface-Enhanced Infrared Spectroscopy (MEIRS) to measure live cells in physiological conditions. In MEIRS, cells are grown on an array of plasmonic nanoantennas called metasurfaces. These resonant nano-antennas support plasmonic hot spots, enhancing the light-matter interaction and IR absorption. We have used MEIRS to detect spectroscopic changes related to cell adhesion and dissociation, cholesterol depletion, response to chemotherapeutics, and activation of intracellular signaling pathways [1-3]. Our current work focuses on expanding the application of MEIRS to mid-infrared chemical imaging, as well as combining plasmonic metasurfaces with nano-topography to study cell-nanostructure interactions. Figure 1 shows a schematic drawing of the MEIRS measurement setup for live cells.

Our mid-IR metasurface is fabricated as an array of gold nanoantennas on IR transparent $CaF_2$ substrates. The substrate is first cleaned using oxygen plasma etcher (Anatech or Glen 1000 Resist Strip) and optionally coated with 20 nm of $SiO_2$ using plasma enhanced chemical vapor deposition (Oxford PECVD) as a protection layer. Metasurface patterns are defined using electron beam lithography with the JEOL 9500 system and poly(methyl methacrylate) (PMMA) as the resist. 5 nm Cr and 70 nm Au are deposited using SC4500 evaporator. If needed, metasurfaces fabricated on large substrates (up to 4" diameter) are diced to smaller pieces using DISCO dicing saw. As the final step, oxygen plasma etcher (Anatech or Glen 1000 Resist Strip) is used to clean the metasurface sample. The metasurface is then attached to superstructures for cell culture chambers and cells are grown on top of the metasurface for analysis. Figure 2 shows a scanning electron microscope image of a cell on the metasurface.

We are currently investigating the mid-IR chemical imaging of cells on the metasurface using a quantum cascade laser (QCL). An inverted laser point-scanning confocal microscope operating in the mid-IR is designed and built, providing a spatial resolution around 5 $\mu$m in the protein absorption bands (amide I and II, 1500 $cm^{-1}$ to 1700 $cm^{-1}$). A hyperspectral image of formalin-fixed cells on the metasurface, with contrast from protein vibrational absorption, is presented in Figure 3. Although the spatial resolution of mid-IR microscopy is lower than visible microscopy, MEIRS microscopy provides chemical contrast in a label-free manner and is suitable for the long-term monitoring of live cells. We plan to apply this MEIRS microscopy to study the localization of different chemical species in live cells and the variation in spectral signature from a heterogeneous population of cancer cells.

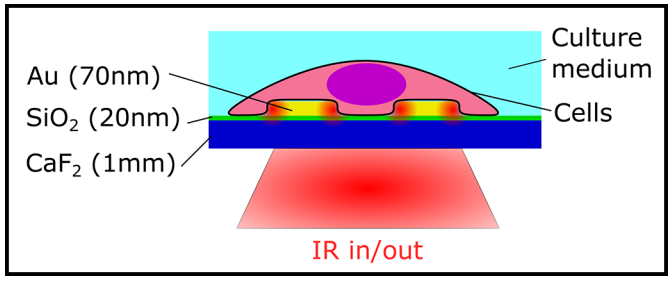


*Figure 1: Schematic drawing of the metasurface-enhanced infrared spectroscopy setup for live cell measurement.*

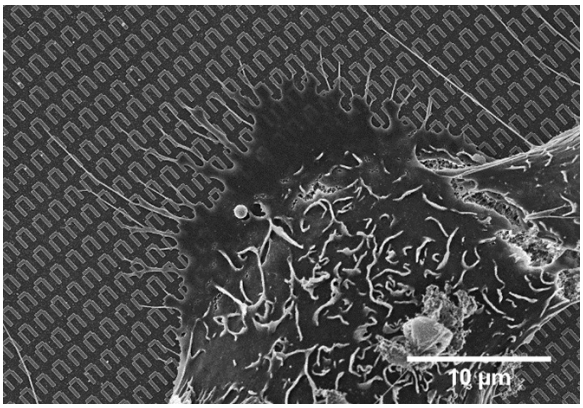


*Figure 2: Scanning electron microscope image of a human skin cancer cell on the metasurface. Scale bar: 10 µm.*

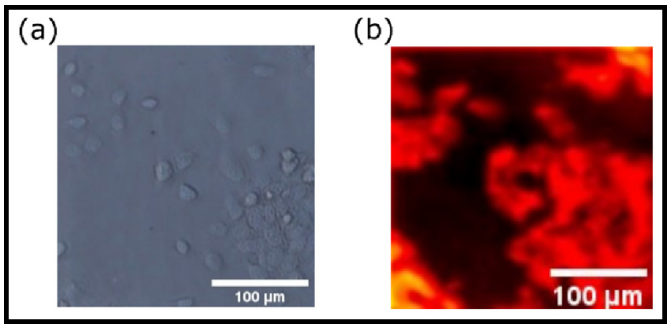


*Figure 3: Formalin-fixed human skin cancer cells on the metasurface. (a) Phase contrast image. (b) MEIRS microscopy image with contrast from protein absorption. Scale bar: 100 µm.*

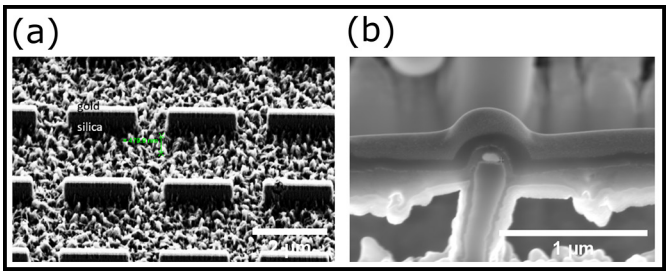


*Figure 4: Nanoantenna-on-nanopillar structure. (a) SEM image of the nanoantenna-on-nanopillar structure without cells. Scale bar: 2 µm. (b) Cross section SEM image of one nanoantenna, with a cell adhered on top. Cell membrane can be seen curved around the nanoantenna-on-nanopillar. Scale bar: 1 µm.*

Another direction in this project is the combination of metasurfaces with nano-topography to study cell-nanostructure interactions. Current research in surface nano-projections has shown that they can be used as effective tools to manipulate cellular attachment. We use nanopillars to incite physical and chemical responses in cells, which are then monitored through MEIRS. We have fabricated gold nanoantennas on top of silica nanopillars (Figure 4(a)). The fabrication process starts with growing a layer of silica (~1$\mu$m) on top of $CaF_2$ substrate using the Oxford PECVD. Next, metasurface patterns are defined using electron beam lithography (JEOL 9500). Gold is deposited in the patterned region using the CVC SC4500 Even/Odd Hour evaporator. We also deposit a thin layer of chromium above the gold nanoantenna and use it as a mask to chemically etch the silica using the Plasma-Therm 740. When cells attach to such nanopillar structures, cell membrane curves around these nanopillars (Figure 4(b)), increasing the overlap between the metasurface hotspots and the cells and also increasing the concentration of certain proteins (actin, clathrin) in the metasurface hotspots. Spectroscopically, we have observed that IR absorption from these cells on the nano-contoured metasurfaces is enhanced and shows different spectral features compared with cells on flat metasurfaces, likely related to protein secondary structures.

## References:

[1] Huang, S. H., et al. Monitoring the effects of chemical stimuli on live cells with metasurface-enhanced infrared reflection spectroscopy. Lab Chip 21, 3991-4004 (2021).

[2] Shen, P.-T., et al. Probing the Drug Dynamics of Chemotherapeutics Using Metasurface-Enhanced Infrared Reflection Spectroscopy of Live Cells. Cells 11, (2022).

[3] Huang, S. H., et al. Metasurface-enhanced infrared spectroscopy in multiwell format for real-time assaying of live cells. Lab Chip 23, 2228-2240 (2023).

# Ultra-Wideband Impedance Spectroscopy of a Live Cell

**CNF Project Number: 2827-19**
**Principal Investigator(s): Alireza Abbaspourrad**
**User(s): Amirhossein Favakeh, Amir Mokhtare**

Affiliation(s): Food Science & Technology, Cornell University

Primary Source(s) of Research Funding: US Army Research, Development and Engineering Command

Contact: alireza@cornell.edu, af446@cornell.edu, am2964@cornell.edu

Primary CNF Tools Used: ABM Contact Aligner, Heidelberg Mask Writer - DWL2000, SC4500 Even-Hour Evaporator

## Abstract:

Accurate measurement of single-cell biophysical properties can represent helpful information on its physiological state. Electrical impedance spectroscopy (EIS) of single cells is a method for quantifying the phenotypic heterogeneity of cells. Compared to conventional optical or biochemical methods, EIS is a fast, compact, label-free, and non-invasive method. Therefore, a single cell can be trapped, characterized, and released using broad microwave frequency, by vector network analyzer (VNA). Hence, the frequency from low (kHz) up to high (GHz) can be swept through the cell to measure the subcellular features of the cell. This data will provide useful information about cell size, membrane properties, cytoplasm, and intracellular properties.

## Summary of Research:

We fabricated a coplanar waveguide (CPW) electrode (Figure 1) that can be set up in a standard microscopy environment [1]. The CPW enables trapping, characterizing, and releasing a single cell and particle. Cells in an isotonic solution are moved through a microchannel equipped with electrodes in an impedance-based microfluidic channel. For this purpose, we fabricated microfluidic channels on these electrodes to guide cells through them at the minimum fluid flow and monitor the cell manipulation inside the channels which only requires one alignment step [2] (Figure 2).

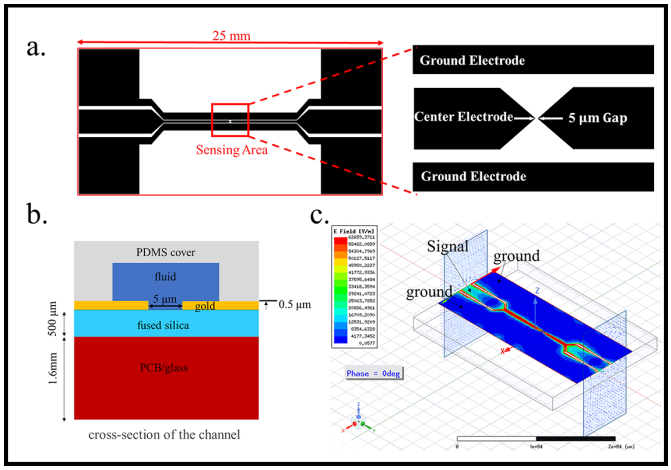


*Figure 1: Coplanar waveguide (CPW) design, that includes a. a gold CPW, 2.5 cm long and 0.5 µm thick, which is deposited on a 500 µm thick fused silica substrate by an e-beam evaporator on a 1.6 mm PCB sheet. The gold CPW was covered with a 5 mm layer of PDMS. A microfluidic channel is molded onto the bottom side of the PDMS cover, intersecting the CPW. There is a 16 µm gap between the center and ground electrodes in the CPW. Besides the electrodes under the microfluidic channel, the center electrode is 200 µm wide. b. CPW cross-sectional dimensions in the channel region. c. The image shows a frequency sweeping pattern between two ports of the electrodes simulated by high-frequency structure simulator (HFSS) software.*

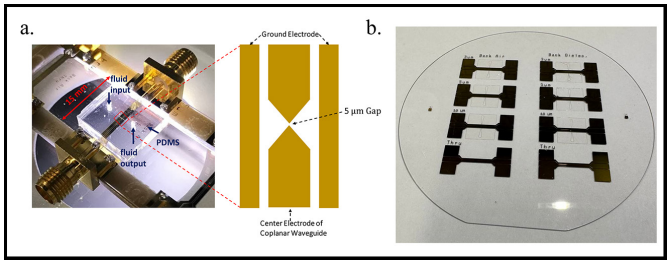


*Figure 2: Microwave microfluidic device, a. The system includes a gold coplanar waveguide covered by PDMS microfluidic channel. b. Shows CPW with a different signal gap.*

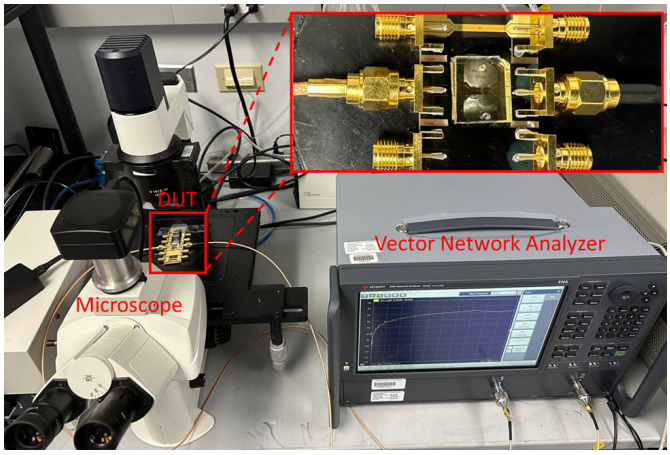


*Figure 3: Shows the experimental setup. The device is placed on the microscope stage and connected to the VNA.*

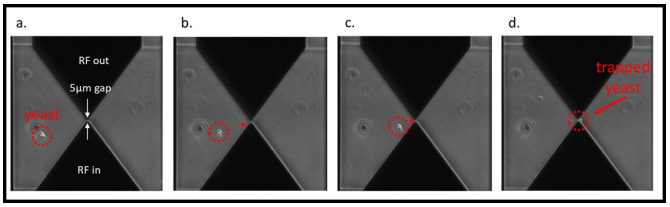


*Figure 4: a-d. Shows single yeast trapped process by DEP micrograph. Yeast can be trapped and released by adjusting the frequency and power of the DEP signal from 5 MHz at 0 dBm to 30 kHz at 3 dBm.*

The experimental setup is shown in Figure 3. We captured the cell using a dielectrophoresis (DEP) signal at 4 MHz and 0 dBm by VNA. The benefits of using this method are that the cells can be captured and released quickly between the two electrodes and the DEP focuses the electric field inside the cell. A yeast cell was trapped in the CPW gap by DEP and visually confirmed using a microscope. A yeast cell moves randomly in solution in the absence of DEP (Figure 4a). When DEP is applied to the solution the yeast is captured and moved toward the electrodes and immobilized by the CPW (Figures 4 b to d). When the cell is trapped between the two sharp electrode points, the majority of the radio frequency (RF) passes through the cell by way of the nucleolus. After trapping the yeast, the VNA was switched from the hold-frequency (4 MHz) to the sweep-frequency mode (30 kHz to 9 GHz) to measure the yeast's biophysical characteristics. The changes in S parameters were calculated and used to derive yeast biophysical characteristics using rapidly successive scattering parameters recorded with and without a trapped yeast.

## Conclusions and Future Steps:

Impedance measurements are frequency dependent such that dispersion of a frequency spectrum can be allocated to different subcellular parts. We developed an ultra-wideband EIS device which is a non-invasive, and label-free method to characterize living single-cells. It can provide helpful information on its physiological state within the radio frequency (RF) range. This enables researchers to analyze the characterization of the cell more efficiently, instead of having to master complex tools.

For future steps, we will test the initially developed CPW electrode for validation and streamlining the sensing measurements. However, coplanar waveguides electrodes, despite having fewer fabrication complications, suffer from electric field non-uniformity with a strong electric field near the electrodes that fades away when moving away electrodes in the vertical direction. We will fabricate vertical electrodes. In this configuration, however, electric field linearity between electrodes is significantly more homogeneous with uniform electric field distribution in the entire testing region. This configuration of electrodes despite having more complexity and fabrication steps, significantly improves measurements' accuracy and signal-to-noise ratio.

## References:

[1] Du, Xiaotian, Caroline Ferguson, Xiao Ma, Xuanhong Cheng, and James C. M. Hwang. 2022. "Ultra-Wideband Impedance Spectroscopy of the Nucleus in a Live Cell." IEEE Journal of Electromagnetics, RF and Microwaves in Medicine and Biology 6 (2): 267-72.

[2] Li, Hang, Caroline Multari, Cristiano Palego, Xiao Ma, Xiaotian Du, Yaqing Ning, Javier Buceta, James C. M. Hwang, and Xuanhong Cheng. 2018. "Differentiation of Live and Heat-Killed E. Coli by Microwave Impedance Spectroscopy." Sensors and Actuators. B, Chemical 255 (February): 1614-22.

# Microfluidic Devices for High-Throughput Directed Evolution of Microbes for Rare Earth Element Purifications

**CNF Project Number: 2852-19**
**Principal Investigator(s): Buz Barstow, Mingming Wu**
**User(s): Sean Medin, Young Joon Suh**

Affiliation(s): Department of Biological and Environmental Engineering, CALS; Cornell University

Primary Source(s) of Research Funding: Air Force Research Labs

Contact: bmb35@cornell.edu, mw272@cornell.edu, sm2769@cornell.edu, ys668@cornell.edu

Primary CNF Tools Used: Heidelberg Mask Writer - DWL2000, ABM Contact Aligner, MVD100, Hamatech Hot Piranha, Class II Photolithography Room

## Abstract:

Rare earth elements (REE), consisting of the lanthanides (elements from lanthanum to lutetium) as well as scandium and yttrium, are important ingredients to many sustainable energy technologies such as magnets — found in hard drives, electric vehicles, and cell phones — room temperature superconductors, and high-efficiency lighting [1]. Current methods for extraction and purification of these elements, however, utilize environmentally harmful chemicals and have a substantial carbon footprint [2]. We aim to use biology to create a cleaner, environmentally sustainable REE purification process. It has been found that bacteria contain numerous sites on their membrane that have specificity for both REE over other elements and for certain REE over other REE [3,4]. We plan on mutagenizing the genome of *V. natriegens* and then doing high-throughput screening to find strains with changes to preference for certain REE over others. We are utilizing the CNF to build a microfluidic droplet generation and sorting device in order to carry out this high-throughput screening.

## Summary of Research:

At the CNF, we used the Heidelberg Mask Writer - DWL2000 to create masks (see Figure 1 for the designs) of our droplet generator and droplet sorter based on the generator and sorter created by Mazutis, et al. [5]. Utilizing the Class II Photoresist room, the Hamatech Hot Piranha, the ABM Contact Aligner, and the MVD100, we used this mask to create a SU-8 mold that we could use to create PDMS devices.

After the creation of these PDMS devices, we bonded them to a glass slide and treated the channels with Aquapel to make them hydrophobic. We then verified that droplets could be formed with this device (Figure 2). We also verified that our bacteria could survive inside these droplets.

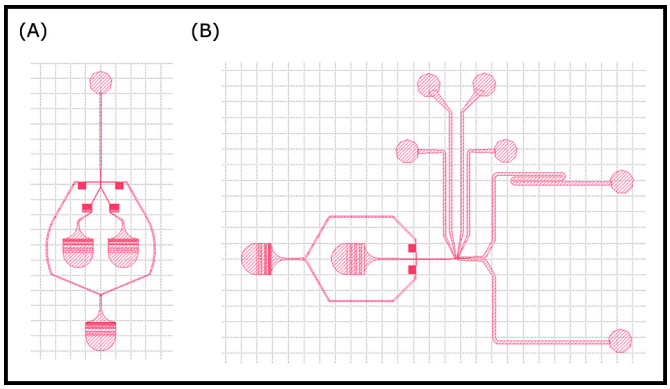


*Figure 1: (A) Droplet generator design. (B) Droplet sorter design.*

While we have yet to fully manufacture the sorting device we created at the CNF — which sorts via electrophoresis and requires the insertion of electrodes into two of the channels — we do have a sample of it created by a company that we were able to test. We verified that we could use this device to sort droplets generated by our device and that the bacteria were able to survive this sorting process that involves applying a square wave with an amplitude of 600-800 volts.

## Conclusions and Future Steps:

Next steps involve integrating the device with an optical system so that we can sort the droplets based on the number of rare earth elements stuck to the bacterial membrane (we have a fluorescent protein that can help us with this). We also need to add electrodes to the sorting device we made at the CNF. Once these steps are done, we will be ready to use our device to select for mutagenized bacteria with membranes that have a preference for particular rare earth elements over others.

*Figure 2: Droplets from droplet generator.*

## References:


[1] Lucas, J., Lucas, P., Le Mercier, T., Rollat, A., and Davenport, W. Rare Earths: Science, Technology, Production and Use. (Elsevier Inc., 2014).

[2] Voncken, J. H. L. The Rare Earth Elements, An Introduction. (2016).

[3] Takahashi, Y., Châtellier, X., Hattori, K. H., Kato, K., and Fortin, D. Adsorption of rare earth elements onto bacterial cell walls and its implication for REE sorption onto natural microbial mats. Chemical Geology 219, 53-67 (2005). https://doi.org:10.1016/j.chemgeo.2005.02.009.

[4] Bonificio, W. D., and Clarke, D. R. Rare-Earth Separation Using Bacteria. Environmental Science & Technology Letters 3, 180-184 (2016). https://doi.org:10.1021/acs.estlett.6b00064.

[5] Mazutis, L., Gilbert, J., Ung, W. et al. Single-cell analysis and sorting using droplet-based microfluidics. Nat Protoc 8, 870-891 (2013). https://doi.org/10.1038/nprot.2013.046.

# Scalable Continuous Flow Electroporation Platform

**CNF Project Number: 2900-20**
**Principal Investigator(s): Thomas Corso**
**User(s): Jacob VanderBurgh**

Affiliation(s): CyteQuest
Primary Source(s) of Research Funding: Investor funding, NIH SBIR Phase I
Contact: tcorso@cytequest.com, jvanderburgh@cytequest.com
Website(s): https://cytequest.com/
Primary CNF Tools Used: Odd-hour evaporator, VersaLaser Engraver/Cutter

## Abstract:

Viral vectors are a bottleneck in the manufacturing of cell therapies. To bypass viral vectors, electroporation has emerged as a non-viral transfection method for primary cells. However, standard cuvette-style approaches are limited by difficult optimization and incompatibility with large-scale cell manufacturing. Here, we present and fabricate a novel electroporation platform that can efficiently transfect small volumes of cells for research and process optimization and scale to volumes required for applications in cellular therapy. We demonstrate delivery of messenger ribonucleic acid (mRNA) to primary human T cells with high efficiency and viability at research scale and we demonstrate seamless scaling of delivery by increasing experimental throughput by a factor of five.

## Summary of Research:

To address limitations associated with cuvette-style electroporation, CyteQuest has developed a scalable electroporation platform to optimize transfection parameters and deliver cargo efficiently and reproducibly at high throughput. Our approach incorporates a single use, continuous-flow fluidic system designed to integrate with automated cell processing approaches. The prototype electroporation flow cell consists of a planar flow chip with a thin slab geometry. It contains a single fluid inlet/outlet that receives cells suspended in electroporation buffer containing the cargo to be delivered. Electrodes are patterned on the top and bottom flow cell surfaces in order to apply a uniform electric field perpendicular to the flow direction (Figure 1A). The thin slab geometry of the device ensures that each cell is subject to the same electric field and the same chemical environment enabling reproducible electroporation. The shallow height (80 $\mu$m) also means that we can achieve the necessary electric field strength to open pores in the cellular and nuclear membranes by applying relatively low voltages (~15 V) compared to the high voltage of traditional commercial systems. The width (2 or 10 mm) of the device is much larger than its depth to allow for rapid and continuous flow of the cells through the chip (Figure 1B). Importantly, the width of the device can be varied to match the desired experimental throughput without changing the electric field experienced by the cells. As such, our planar geometry enables us to seamlessly scale from small volumes of precious sample to determine optimal transfection parameters to large volumes for delivery at clinical scales.

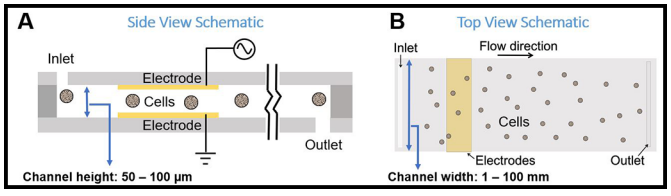


*Figure 1: (A) Side view schematic of the flow cell (not to scale). (B) Top view schematic of the flow cell (not to scale).*

Electroporation flow chips are constructed from a three-layer stack of polymer substrates. All three layers are laser cut with a small beam spot, high resolution carbon dioxide laser produced by the VersaLaser Engraver/Cutter. The top and bottom layers, cut from 1 mm thick acrylic slabs, create the floor and sealing channel surfaces. The middle layer is a spacer that defines the channel depth and width and is composed of a thin pressure sensitive adhesive tape. To fabricate the chip, the bottom and top acrylic layers are laser-cut into 1" × 2" pieces. The pieces are then laser-cut to add fluid inlet/outlet ports and alignment holes for use during the assembly process. Afterwards, a thin film electrode of gold is deposited by physical vapor deposition on the inside surface of each acrylic piece at the Cornell NanoScale Facility (CNF) using the odd-hour evaporator. The middle layer is cut to shape and also receives the corresponding alignment holes via the laser cutting process. The three-piece (acrylic, spacer, acrylic) sandwich assembly is then compression bonded in a press.

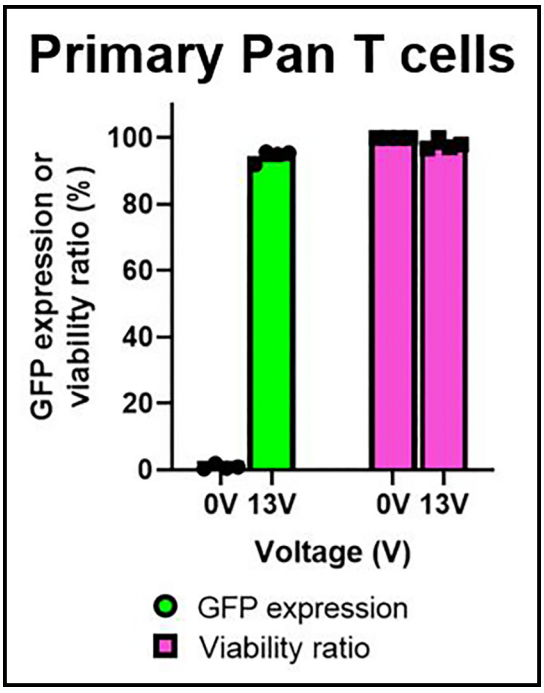


*Figure 2: Delivery of mRNA to primary human T cells. Data from primary T cells from four healthy donors (n = 4). Data shown as mean ± standard deviation.*

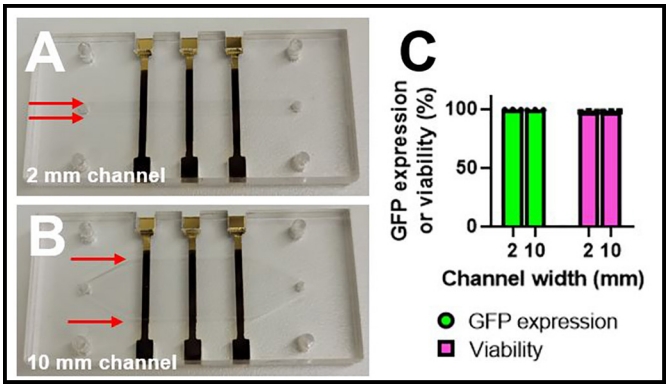


*Figure 3: Scaled-up delivery of mRNA to Jurkat cells. (A) Photograph of a 2 mm and (B) 10 mm electroporation flow cell. Red arrows highlight the channel width. (C) Plot of GFP expression and viability values from Jurkat cells transfected with mRNA encoding GFP in either the 2- or 10-mm channels (n = 3). Data shown as mean ± standard deviation.*

Cells with the cargo to be transfected are loaded into a syringe and injected through tubing into the flow cell by a syringe pump. As cells flow through the electrode pair, they experience a spatially uniform electrical field produced by a computer-controlled function generator and amplifier. The applied voltage waveform and resultant current are monitored via an oscilloscope. The electroporated cells then exit the flow cell and are dispensed into wells of a well-plate by a robotic fraction collector. Computer-controlled waveform selection and robotic sampling enable rapid sweeping of waveform parameters such as the voltage amplitude or waveform shape.

Using this system, CyteQuest has delivered mRNA encoding green fluorescent protein (GFP) to primary human T cells with high efficiency and high viability, observing > 95% transfection efficiency with < 2% loss of cell viability compared to control cells (Figure 2). To demonstrate the ability of our device to scale experimental throughput, we increased the width of the device from 2 to 10 mm and the volumetric flow rate from 320 $\mu$L/min to 1.6 mL/min (Figure 3A-B). Scaling both the channel width and flow rate by a factor of five produced identical GFP expression and viability values in both channel widths for Jurkat cells transfected with mRNA encoding GFP (Figure 3B). Overall, these data demonstrate the ability of our platform to efficiently deliver mRNA to cells and seamlessly scale-up delivery without changing delivery performance.

# Investigating the Effect of the Tumor Microenvironment on Metastatic Progression Using Micro and Nano-Scale Tools

**CNF Project Number: 2912-20**
**Principal Investigator(s): Claudia Fischbach**
**User(s): Matthew Tan, Nicole Sempertegui**

Affiliation(s): Biomedical Engineering, Cornell University

Primary Source(s) of Research Funding: Stem Cell Research Training Fellowship, Stem Cell Program of Cornell; Center on the Physics of Cancer Metabolism Award Number 1U54CA210184-01, National Cancer Institute

Contact: cf99@cornell.edu, mlt239@cornell.edu, nds68@cornell.edu

Primary CNF Tools Used: ABM Contact Aligner, Heidelberg DWL2000, Hamatech 9000, Malvern NS300 NanoSight

## Abstract:

Breast cancer mortality is driven by metastasis, where cancer cells disseminate from the primary tumor to seed distant tissues. During the metastatic cascade, cancer cells interact with their microenvironment consisting of extracellular matrix including collagen and other cell types such as endothelial cells in blood vessels and macrophages in the bone. Cancer cells may interact locally with these cells in the primary tumor microenvironment or from distant sites in the body through soluble factor signaling. In this study, CNF tools were used to investigate the two stages in metastasis: early invasion of tumor cells towards blood vessels and tumor cell invasion into the bone to form a pre-metastatic niche. For the former, we developed a microfluidic model of the perivascular niche and found that ECs stimulate breast cancer invasion into collagen, and that an EC-coated microchannel exhibits a distinct diffusion profile from a channel without ECs. For the latter, the same microfluidic model was modified to incorporate collagen mineralization to mimic bone ECM. Using this model, we have shown that tumor cell invasion is inhibited when co-cultured with macrophages seeded in a mineralized microchannel. Future work will continue to use the microfluidic model to investigate the mechanisms by which ECs influence cancer invasion and how mineralized collagen affects cancer cells and the formation of a pre-metastatic niche.

## Summary of Research:

**Introduction.** Breast cancer is the second leading cause of cancer-related death for women in the United States [1]. Mortality in breast cancer is driven by metastasis, where tumor cells disseminate from the primary tumor and spread to distant tissues. During this process, tumor cells become invasive and move towards blood vessels, where they will enter the circulation and seed onto distance sites such as the bone. Tumor cells that proceed through the metastatic cascade encounter a changing microenvironment consisting of extracellular matrix (ECM) such as collagen and other cell types, including endothelial cells (ECs) and macrophages [2]. These cells are known to participate in reciprocal signaling with tumor cells to influence tumorigenesis through the exchange of soluble factors [2,3]. However, the mechanisms by which soluble factor signaling influence tumor cell invasion and the development of a pro-tumorigenic microenvironment remain unclear due to the lack of models that enable systematic study. To this end, we have used the expertise at the CNF to investigate two key steps in the metastatic cascade: initial invasion towards ECs in blood vessels, and later stage invasion into the bone pre-metastatic niche.

**Regulation of Breast Cancer Invasion Using a Microfluidic Model of the Perivascular Niche.** In early invasion, tumor cells initially invade towards blood vessels, responding to metabolic gradients from the vessels and signaling gradients from ECs. Using SU-8 photolithography in conjunction with the ABM Contact Aligner and a photomask generated by the Heidelberg DWL2000, we have created a dual channel microfluidic devices that enables co-culture of breast cancer cells and ECs encapsulated in a 3D collagen matrix. In this system, we found that the presence of ECs stimulated cancer invasion into a collagen hydrogel (Figure 1). Additionally, using fluorescent molecule diffusion studies, we found that an EC-coated channel restricted diffusion of molecules within in the channel compared to a channel without ECs (Figure 2).

**Effects of Mineralized Collagen on Breast Cancer Cell Invasion Using a Microfluidic Model of the Bone Pre-Metastatic Niche.** To colonize bone, disseminated tumor cells extravasate from the vessel and invade through the bone marrow to seed osteogenic niches [4]. Tumor cell invasion during this process is controlled by host cells including macrophages. Macrophages are particularly relevant as they not only exert immunomodulatory effects, but also have the potential to differentiate into

osteoclasts, the primary cell type driving osteolysis in bone metastasis patients. To model these interactions within a bone-like microenvironment, the microfluidic device described above was modified using the polymer-induced liquid precursor (PILP) method to include a mineralized collagen microchannel [5]. In this model, the mineralization of collagen, the primary component of bone matrix, as well as tumor cell and macrophage seeding can be selectively controlled. We have shown that macrophages promote the invasion of breast cancer cells regardless of collagen mineralization and that this effect occurs without cell-cell contact, suggesting that it was caused by soluble factors secreted from macrophages. It was also determined that collagen mineralization inhibits the ability of macrophages to promote tumor cell invasion (Figure 3).

## Conclusions and Future Steps:

In this project we were able to develop tools and pipelines to study the breast cancer metastatic cascade. We were able to successfully fabricate and culture a 3D microfluidic tumor-perivascular niche model. Future work using this device will uncover the metabolic and mechanical mechanisms by which ECs influence breast cancer invasion. We were also able to isolate and characterize breast cancer derived ECs. Additionally, the 3D microfluidic device was modified to recapitulate key microenvironmental features of the bone pre-metastatic niche. These studies have shown that this model system is highly adaptable and can be modified by introducing additional cell types and/or soluble factors to probe other aspects of bone and tumor cell interactions. Future work includes will characterize the mineralized collagen and validate findings with primary murine bone marrow-derived macrophages.

## Funding Acknowledgements:

Stem Cell Research Training Fellowship, by the Stem Cell Program of Cornell(NS). The work described was supported by the Center on the Physics of Cancer Metabolism through Award Number 1U54CA210184-01 from the National Cancer Institute. The content is solely the responsibility of the authors and does not necessarily represent the official views of the NCI or the NIH.

## References:

[1] Siegel, R. L., Miller, K. D., Fuchs, H. E., and Jemal, A. Cancer Statistics, 2021. CA. Cancer J. Clin. 71, 7-33 (2021).

[2] Tan, M. L., Ling, L., and Fischbach, C. Engineering strategies to capture the biological and biophysical tumor microenvironment *in vitro*. Adv. Drug Deliv. Rev. 176, 113852 (2021).

[3] Zheng, P., and Li, W. Crosstalk Between Mesenchymal Stromal Cells and Tumor Associated Macrophages in Gastric Cancer. Front. Oncol. 10, 1-9 (2020).

[4] Peinado, H., et al. Pre-metastatic niches: organ-specific homes for metastases. Nat. Rev. Cancer 17, 302-317 (2017).

[5] Choi, S., et al. Intrafibrillar, bone-mimetic collagen mineralization regulates breast cancer cell adhesion and migration. Biomaterials. 198, 95-106 (2019).

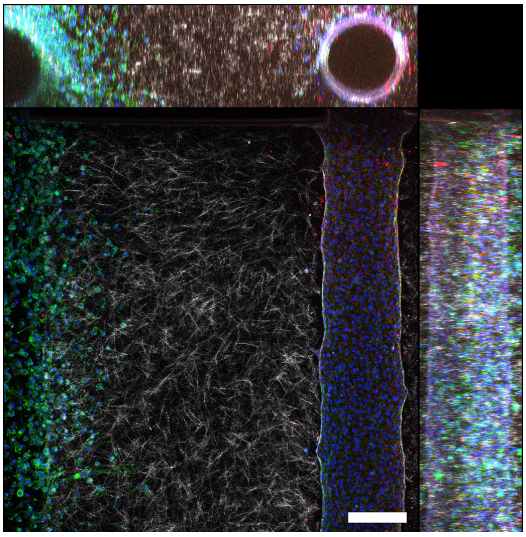

*Figure 1: Confocal microscopy projection of breast cancer cells invading towards an endothelial cell channel stained with CD31 (red). DAPI was used to stain nuclei (blue), phalloidin was used to stain f-actin (green), and confocal reflectance was used to visualize collagen fibers (white). Scale bar: 200 µm.*

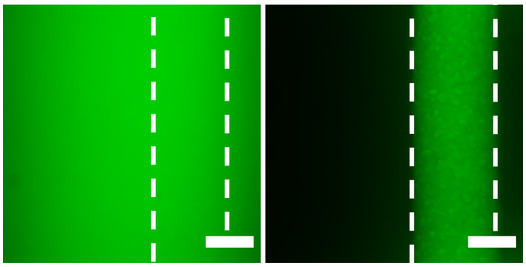

*Figure 2: Diffusion of fluorescein (FITC) from a non-human umbilical vein endothelial cell (HUVEC) channel and a HUVEC coated channel. Scale bar: 200 µm.*

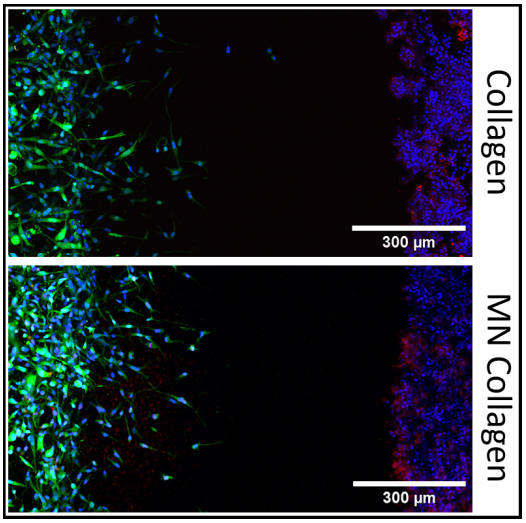


*Figure 3: Fluorescent max intensity projection of non-mineralized collagen device (top) and mineralized (MN) collagen device (bottom) seeded with MDA-MB-231 breast cancer cells (green) and RAW264.7 macrophage cells (red). DAPI was used to stain nuclei (blue) Scale bar: 300 µm.*

# Fabrication of a Nanofluidic Fabry-Perot Cavity

**CNF Project Number: 3069-23**
**Principal Investigator(s): Ronald Koder**
**User(s): Paul Molinaro**

Affiliation(s): Department of Physics, City College of New York
Primary Source(s) of Research Funding: NSF MCB-2025200, NYSERDA NYS115213
Contact: rkoder@ccny.cuny.edu, pmolinaro@ccny.cuny.edu
Website(s): https://www.koderlab.org/
Primary CNF Tools Used: Mask Aligner, Substrate Bonder

## Abstract:

Nanofluidic Fabry-Pérot cavities allow well understood experimental techniques from condensed matter physics to be applied to photoactive proteins under biological conditions [1]. Previous attempts to probe photoactive proteins with these techniques required the encapsulation of the system into a polymer [2] or the creation of a dehydrated thin film [3], significantly altering the proteins from their natural form. Recently, a method for measuring the reorganization energy via strong coupling to a Fabry-Pérot cavity has been proposed [4]. Due to the wavelengths involved in photo excitation, the height of these cavities must be on the order of 100 nm. These cavities can only be loaded nanofluidicly. Bahsoun and collaborators have recently fabricated a nanofluidic Fabry-Pérot cavity suitable for this experiment [1]. Our fabrication strategy borrows heavily from their approach. We are using the resources provided by the Cornell NanoScale Science and Technology Facility (CNF) to fabricate a nanofluidic Fabry-Perot Cavity.

## Summary of Research:

Our lab is engaged in the design and engineering of new photosynthetic proteins [4]. Electron transfer in biological systems is well described by Marcus Theory [5]. The reorganization energy ($\lambda$) is crucial to predicting the rate of electron transfer for a given process. The parameter is most easily measured by measuring the rate of transfer as a function of the driving force of the reaction. Within a Fabry-Perot cavity, the energy of the donor state, and by extension the free energy of electron transfer, can be controlled by the number of molecules in the cavity. This observation suggests measuring the transfer rate as a function of concentration is equivalent to measuring a Marcus curve, from which $\lambda$ can be extracted. The electron transfer rate can be measured by fabricating two cavities with an equal number of coupled molecules. In one cavity, the electron acceptor is absent. The reduction in transmission intensity in the presence of an electron acceptor is due to electron transfer.

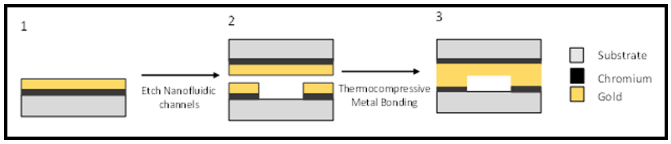


*Figure 1: The nanofluidic cavity fabrication strategy. First metal is deposited on a substrate, then channels are etched into the metal via a lithographic process and two chips are bonded together by thermocompressive gold bonding.*

An outline of our fabrication strategy is shown in Figure 1. A 100 mm glass wafer is coated with a 5 nm layer of chromium and between 250-500 nm of gold. A roughly 2 $\mu$m layer of AZ1512 photoresist is deposited via spin coating and baked at 110°C for 1 minute. The channels are patterned into the photoresist by exposing the resist to 150 mJ of UV light and baked for an additional minute. Development takes place by submerging the wafer in AZ 300 MIF developer for ~ 35 seconds. The exposed gold and chromium are etched away by submersion in Transene gold TFA etchant and chromium 1020 etchant for an amount of time dictated by the thickness of each metal layer. The remaining photoresist is stripped by soaking the wafer in acetone for two minutes with constant agitation. The wafers are then washed twice with methanol, isopropanol and deionized water before being blown dry with nitrogen. The wafer is then diced

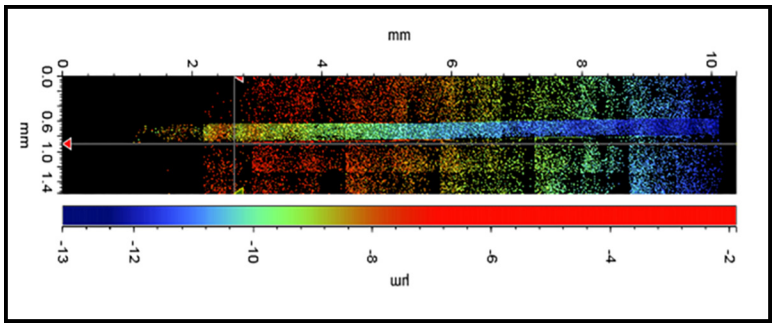


*Figure 2: The depth of the cavity across the length of the channel, showing significant depth changes from one end of the channel to the other.*

into 10 mm × 10 mm chips. Immediately before bonding, the washing step is repeated followed by a 2-minute 200-watt oxygen plasma ashing. One patterned chip and an unpatterned chip are aligned in a custom machined stainless-steel plate and another plate is hand screwed on top to apply pressure. The entire set-up is heated to 350°C for 30 minutes under a vacuum. Once the apparatus is cooled, the finished chip is removed.

So far, none of the finished chips have been wettable. This is due to the uneven application of pressure applied by the two steel plates. A depth profile of the resulting cavity can be seen in Figure 2. The cavity is of non-unform depth, a quality that is known for impeding nanofluidic flow.

## Conclusion and Future Steps:

Currently, thermocompressive gold bonding is carried out using a custom, home built apparatus. We have been unable to produce a smooth enough surface to apply uniform pressure and thus create cavities of uniform depth. The thermocompressive gold bonding will no longer be performed using a hand screwed apparatus. Instead, a SUSS SB8e substrate bonder will be used to carry out the bonding. The tool allows for controlled, uniform application of pressure as well as temperature and pressure ramping. Once the bonding process is optimized, the cavities will be loaded with the photoactive substrate of interest and the reorganization energy will be measured.

## References:

[1] Bahsoun, H., Chervy, T., Thomas, A., Börjesson, K., Hertzog, M., George, J., Devaux, E., Genet, C., Hutchison, J.A., Ebbesen, T.W., 2018. Electronic Light-Matter Strong Coupling in Nanofluidic Fabry-Pérot Cavities. ACS Photonics 5, 225-232. doi:10.1021/acsphotonics.7b00679

[2] Wu, F., Finkelstein-Shapiro, D., Wang, M., Rosenkampff, I., Yartsev, A., Pascher, T., Nguyen- Phan, T.C., Cogdell, R., Börjesson, K., Pullerits, T., 2022. Optical cavity-mediated exciton dynamics in photosynthetic light harvesting 2 complexes. Nature Communications 13. doi:10.1038/s41467-022-34613

[3] Satapathy, S., Liu, B., Deshmukh, P., Molinaro, P.M., Dirnberger, F., Khatoniar, M., Koder, R.L., Menon, V.M., 2022. Thermalization of Fluorescent Protein Exciton-Polaritons at Room Temperature. Advanced Materials 34, 2109107. doi:10.1002/adma.202109107

[4] Mauro, L., et al. "Charge-transfer chemical reactions in nanofluidic Fabry-Pérot cavities." Physical Review B 103.16 (2021): 165412.

[5] Mutter, A. C.; Norman, J. A.; Tiedemann, M. T.; Singh, S.; Sha, S.; Morsi, S.; Ahmed, I.; Stillman, M. J.; Koder, R. L., Rational Design of a Zinc Phthalocyanine Binding Protein Journal of Structural Biology 2014, 185 (2), 178-185.

[6] Punnoose, A.; McConnell, L. A.; Liu, W.; Mutter, A. C.; Koder, R. L., Fundamental Limits on Wavelength, Efficiency and Yield of the Charge Separation Triad. PLoS One 2012, 7(6).